Twelfth Australasian Fluid Mechanics Conference
The University of Sydney, Australia 1995

VISCOELASTIC FLOW BETWEEN ECCENTRIC ROTATING CYLINDERS BY UNSTRUCTURED CONTROL VOLUME METHOD

X. Huang, N. Phan-Thien and R.I. Tanner
Mechanical & Mechatronic Engineering Department
The University of Sydney
Sydney, New South Wales
Australia

ABSTRACT

This paper reports a convergent numerical algorithm for the Upper-Convected Maxwell (UCM) fluid between two eccentric cylinders at various eccentricity ratios (ϵ); the outer cylinder is stationary, and the inner one rotating. The problem is solved by an unstructured control volume method (UCV), which is designed for a general viscoelastic flow problem with an arbitrary computational domain. A self-consistent false diffusion technique and a domain iteration scheme are used in combination to solve the problem. The computations of the UCM fluid using the numerical algorithm are carried out to a higher value of the Deborah number (De) at each eccentricity tested than hitherto possible with previous numerical simulations. The solutions are compared with previous numerical results, confirming the effectiveness of the UCV method as a general technique for solving viscoelastic flow problems.

GOVERNING EQUATIONS

We consider a general two-dimensional and isothermal flow of the UCM fluid, where the governing equations are the mass and momentum conservation,

$$\nabla \cdot \mathbf{u} = 0, \quad -\nabla p + \nabla \cdot \boldsymbol{\tau}_1 + \eta_0 \nabla^2 \mathbf{u} = 0, \quad (1)$$

and the constitutive equations,

$$\boldsymbol{\tau}_1 + \lambda \frac{D\boldsymbol{\tau}_1}{Dt} = -\lambda \frac{D\boldsymbol{\tau}_2}{Dt}, \quad (2)$$

$$\frac{D\boldsymbol{\tau}_i}{Dt} = \frac{\partial \boldsymbol{\tau}_i}{\partial t} + \mathbf{u} \cdot \nabla \boldsymbol{\tau}_i - \nabla \mathbf{u}^T \cdot \boldsymbol{\tau}_i - \boldsymbol{\tau}_i \cdot \nabla \mathbf{u}$$

$$\boldsymbol{\tau}_2 = \eta_0 (\nabla \mathbf{u} + \nabla \mathbf{u}^T),$$

where $\boldsymbol{\tau}_1$ and $\boldsymbol{\tau}_2$ are non-Newtonian and Newtonian contributions to the total extra stress $\boldsymbol{\tau} = \boldsymbol{\tau}_1 + \boldsymbol{\tau}_2$, respectively, $\mathbf{u} = \{u, v, w\}$ is the velocity field, η_0 is a constant viscosity, and λ is the relaxation time. The constitutive equation is the familiar Upper Convective Maxwell (UCM) model. There is no good physical reason for choosing this particular constitutive equation, but it has been recognised that any scheme that can deal effectively with this (numerically) difficult constitutive equation must necessarily be robust and should do well with other less demanding constitutive equations. The UCM constitutive equation is written here in an operator splitting form, first introduced by Perera and Walters (1977). This form is used in the present control volume scheme since it explicitly introduces a viscous stress into the momentum equation.

The problem to be considered here is the annular flow between two eccentric cylinders of radii R_i (inner cylinder) and R_o (outer cylinder), offset by a centre-to-centre distance of e. Distances will be made dimensionless with respect to R_i. We define the dimensionless *gap*

$$\mu = (R_o - R_i) / R_i,$$

and the *eccentricity ratio*

$$\epsilon = e / (R_o - R_i).$$

In the iteration process, the same pseudo-diffusion terms are added to both sides of the constitutive Eq. (2), the effects of which vanish as the algorithm converges to a steady state solution;

Equation	Φ	Λ	Γ	S_Φ
continuity	1	ρ	0	0
momentum	$\mathbf{u}$	ρ	η_0	$-\nabla p + \nabla \cdot \boldsymbol{\tau}_1$
constitutive	$\boldsymbol{\tau}_1$	λ	0	$-\lambda D\boldsymbol{\tau}_2/Dt - \boldsymbol{\tau}_1 + \lambda(\nabla \mathbf{u}^T \cdot \boldsymbol{\tau}_1 + \boldsymbol{\tau}_1 \cdot \nabla \mathbf{u})$

Table 1: Definitions of variables.

they are however treated differently: terms on the right hand side are considered to be sources, and terms on the left hand side participate in the finite volume discretisation process. All of the governing equations can now be written as a general transport equation in the form

$$\nabla \cdot (\Lambda \mathbf{u}\Phi - \Gamma \nabla \Phi) = S_P \Phi + S_c, \qquad (3)$$

or

$$\nabla \cdot \mathbf{J} = S_\Phi, \qquad (4)$$

where $\mathbf{J}$ is the "flux" of the variable Φ, and S is the source term, which can be arbitrarily split up in the manner shown in Eq. (3). The definition of different variables can be found in Table 1 (with no false diffusion terms in the constitutive equations).

NUMERICAL METHOD

The SIMPLER algorithm Patankar (1980) is by far the most popular finite volume method to solve conservation equations of the form (3), especially for Newtonian flows at moderate to high Reynolds numbers. The method and its modifications are becoming attractive in numerical viscoelastic flows. We here adopt the SIMPLER algorithm, but apply it to an unstructured non-staggered mesh. This is a key development that has apparently not been successfully done before. In the unstructured mesh, there are no obvious lines to march the solution along; however, the basic structure of the line-by-line algorithm is kept by introducing an automatic sweeping line generating algorithm, which searches and creates lines of nodes from the entry to the exit boundaries. If this is not possible, then the line is terminated in the domain. The information thus generated is stored in a sweeping line array. Similar to a re-ordering of the nodes in the FEM to minimize the bandwidth of the system matrix, this array stores all the information needed for the line-by-line tridiagonal-matrix algorithm (TDMA), which only requires computer storage and computer time of $O(N)$, where N is the number of unknowns. The line-by-line method is faster than a point by point solver (provided that the problem converges), partly because the boundary condition information is transmitted quickly to the interior of the domain. After a discretisation of the flow domain into non-

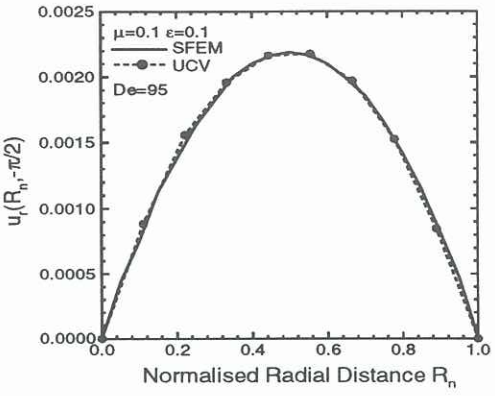

Figure 1: Radial velocity for the UCM fluid with $\epsilon = 0.1$, $\mu = 0.1$ (SFEM, solid lines), together with the UCV results (squares) at $De = 95$. The calculations were done on a mesh with 10 radial elements.

overlapping polygon control volumes that surround the nodes in the flow domain, a connectivity array is constructed to identify each grid point and its neighbours, denoted by P and the subscript nb, respectively.

The final discretisation equation for the variable Φ

$$a_P \Phi_P = \sum a_{nb} \Phi_{nb} + b, \qquad (5)$$

where

$$b = S_c \Delta V,$$

$$a_P = \sum a_{nb} - S_P \Delta V,$$

in which the summation is to be taken over all the neighbouring nodes.

In a similar manner, the discretisation equation for pressure is obtained by using the discretised continuity equation in the discretised momentum equation with a different set of coefficients a_P, a_{nb} and b. These discretised equations are solved sequentially, using the TDMA solver along the sweeping lines.

NUMERICAL RESULTS

In the flow of the UCM fluid between eccentric rotating cylinders, all the distances are made dimensionless with respect to R_i, velocities with ωR_i, and stresses with $\eta_0 \omega$. The definition of the Deborah number, which is a measure of the level of elasticity in the flow, is defined by

$$De = \lambda \omega$$

The normalised dimensionless radial distance R_n is defined as

$$R_n = \frac{R - R_i}{R_o - R_i} (1 + \epsilon \cos\theta)$$

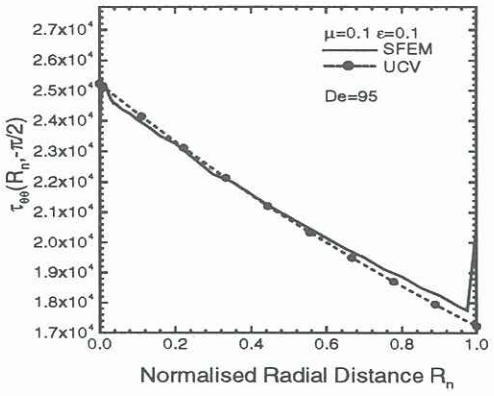

Figure 2: Azimuthal stress $\tau_{\theta\theta}$ for the UCM fluid with $\epsilon = 0.1$, $\mu = 0.1$ (SFEM, solid lines), together with the UCV results (squares) at $De = 95$. The calculations were done on a mesh with 10 radial elements.

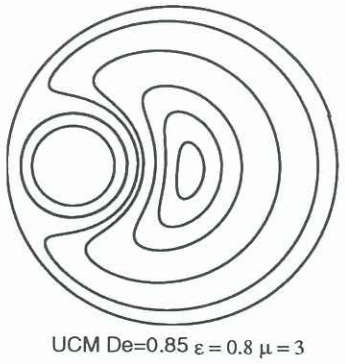

Figure 3: Streamlines for the UCM fluid with $De = 0.85$, $\epsilon = 0.8$, and $\mu = 3$. The calculations were done on a mesh with 33 radial elements.

where R is the radial distance and θ is the azimuthal angle; R_n is to be used for plotting only. The algorithm is first benchmarked against the Newtonian solution in the eccentric geometry, and the UCM solution in the concentric geometry (circular Couette flow). In both cases, a convergence to the exact solution with mesh refinement is demonstrated, with the convergence rate estimated at $O(h^2)$ for velocities, $O(h^1)$ for extra stresses where h is a measure of the mesh size. Obviously, our UCV code has reached the standard error bounds for linear FEM. For the UCM case in the circular Couette geometry, convergence is obtained up to a Deborah number of 100.

We consider next the flow of the UCM fluid at an eccentricity ratio of $\epsilon = 0.1$, and dimensionless gap $\mu = 0.1$, for which reliable numerical data is available by the spectral/finite element and the perturbation method. Figures 1 and 2 show the radial velocity u_r and the azimuthal stress $\tau_{\theta\theta}$ up to $De = 95$ along the line $\theta = -\pi/2$.

Our numerical data agree well with the spectral/finite element results except for the stress boundary layer found by Beris *et al.*(1987). Our scheme failed to predict such a boundary layer (a sharp drop of the stress at the inner cylinder, and a sharp increase of the stress at outer cylinder across a boundary layer thickness of less than 1% of the radial gap) for this geometry. Much more refinement along the radial direction is needed to capture such a boundary layer. The boundary stresses are calculated by integrating a set of ordinary differential equations along the boundary, where the only kinematic term that needs updating is $\partial u_\theta/\partial r$. The calculations were done by a trapezoidal scheme, and although only 10 control volumes are used in the radial direction, we believe that the boundary stresses are calculated accurately from the given kinematics. In Figures 1 and 2 SFEM results were calculated on a mesh which has 200 radial elements Beris *et al* (1987). The current scheme requires the same order of refinement in both the azimuthal and the radial directions to ensure a reasonable aspect ratio of the control volumes. To achieve the same order of refinement as in the SFEM would require considerably more computing time and memory storage. We have doubled the number of radial elements and obtained visually identical results. A search for stress boundary layers is made by a combination of the UCV method and numerically integration of the stresses along the boundaries. The calculated results show that the boundary stresses are quite accurate indeed. The details have been reported in another paper.

Furthermore, the algorithm is most robust: we continue to obtain convergence up to a Deborah number of $O(102)$; whereas the spectral method ceased to converge at $De = O(95)$, and the finite element calculation at $De = O(8)$, for the same flow configuration.

Numerical calculation was also done on a large dimensionless gap $\mu = 3$ for which no previous numerical results are available. On this geometry the re-circulation region is enhanced by the large μ. The calculations were done on a mesh with 33 elements along the radial direction, and converged solutions were obtained at De of order 2, with the final size of the diffusivity of 0.01% of De. (The highest Deborah number for which convergent solutions were obtained with the SFEM at this eccentricity, but with $\mu = 0.1$, was $De = 0.85$ (Beris *et al* (1987)).

Figure 3 displays the streamlines at $De = 0.85$.

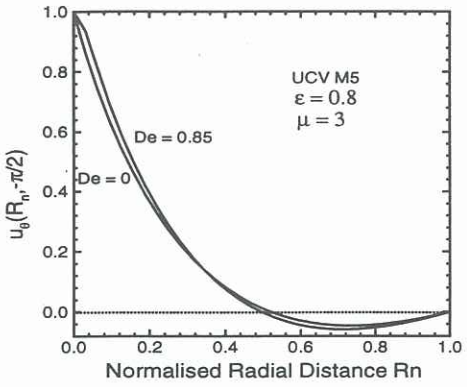

Figure 4: Radial velocity for the UCM fluid with $\epsilon = 0.8$, $\mu = 3$, and $De = 0.85$. The calculations were done on a mesh with 33 radial elements.

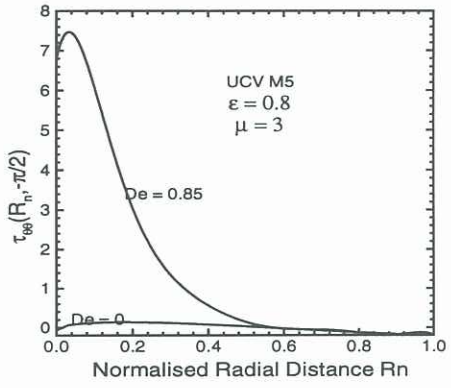

Figure 5: Azimuthal stress $\tau_{\theta\theta}$ for the UCM fluid with $\epsilon = 0.8$, $\mu = 3$, and $De = 0.85$. The calculations were done on a mesh with 33 radial elements.

The primary feature of the flow is a recirculation region, which is seen to dominate most of the flow domain.

The azimuthal velocity u_θ and the normal stress $\tau_{\theta\theta}$ are plotted against normalised radial distances R_n along the line $\theta = -\pi/2$ in Figures 4–5. We note that the extra stress $\tau_{\theta\theta}$ varies rapidly with De, even for small changes in De. The region of high stress is confined to a region near to the inner cylinder as shown in Fig 5. In this region the stress gradients are higher than the corresponding values in the re-circulation region.

FINAL REMARKS

The results of the unstructured finite volume calculations presented here are rather encouraging for computations of complex flow with arbitrary geometry. The unstructured nature of the algorithm alows us to handle more complex geometry than presented here, in much the same way as the FEM. Yet the numerical oscillations observed in FEM solution at high Deborah are absent from the current UCV calculation, and in fact converged solutions are obtained at much higher Deborah numbers than have been successfully reached by FEM calculations.

Our results also compare favourably with those obtained with the SFEM, which is specifically designed for the eccentric cylinder problem (and therefore lacks the flexibility required for general flow problems), in terms of the quality of the solution and the limiting Deborah number reached. To resolve the issue of the stress boundary layer at low eccentricity ratio, a much more refined mesh needs to be used, and this has been investigated in another paper.

The support provided by an Australian Research Grant is gratefully acknowledged.

REFERENCES

Perera, M.G.N. and Walters, K., 1977 "Long-range memory effects in flows involving abrupt changes in geometry." *J. non-Newt. Fluid Mech.*, vol. 2, pp. 49–81.

Beris, A.N., Armstrong, R.C. and Brown, R.A., 1987 "Spectral/finite-element calculations of the flow of a Maxwell fluid between eccentric rotating cylinders." *J. non-Newt. Fluid Mech.*, vol. 22, pp. 129–167.

Patankar, S.V., 1980 *Numerical Heat Transfer and Fluid Flow*, Hemisphere Publishing Corporation, New York.